J Mater Sci (2007) 42:9421–9428
DOI 10.1007/s10853-007-1867-4

# Characterization of Zr-doped $TiO_2$ prepared by homogenous co-precipitation without high-temperature treatment

**Jozef Lukáč · Mariana Klementová · Petr Bezdička · Snejana Bakardjieva · Jan Šubrt · Lórant Szatmáry · Anna Grusková**

Received: 16 February 2006 / Accepted: 21 May 2007 / Published online: 27 July 2007


**Abstract** Zr-doped $TiO_2$ (anatase) was prepared by the homogenous co-precipitation method of the aqueous solutions containing $TiOSO_4$ and $ZrCl_4$ using urea as the precipitation agent. Nanocrystallites of Zr-doped $TiO_2$, 6–9 nm in size, intergrown with amorphous phase form 1–2 μm porous spherical clusters. Crystallite size of anatase decreases with increasing Zr content, and the catalyst becomes totally amorphous at 10 mol.% Zr. All samples exhibit high specific surface area, which increases with the addition of zirconium (from 391.3 to 689.1 $m^2\ g^{-1}$).

## Introduction

Titanium dioxide has a wide range of applications due to its excellent physical and chemical properties, for example as white pigment, in cosmetics or catalyst carrier. Furthermore, it is used as semiconductor with photocatalytic activities with applications in environmental purification, decomposition of carbon dioxide or hydrogen generation. Metal oxides, such as $ZrO_2$ or $TiO_2$, modified with sulphate, develop strong acidity, and act as a potential catalyst for low temperature isomeration, esterification, alkylation and cracking reactions. Sulphate-promoted zirconium oxide became a centre of investigation due to its high thermal and mechanical stability, low reducibility as well as the lower reactivity with respect to the active phases. It is well known that the chemical and physical properties of Zr-doped $TiO_2$ are significantly influenced by the preparation method and calcination temperature [1]. All microstructural parameters, such as particle shape and size, specific surface area and porosity are quite sensitive to pH, metal ion concentration, temperature and aging time [2].

Daly et al. [3] prepared samples of $TiO_2$–$ZrO_2$ by calcination of hydroxides at 300–700 °C. The co-precipitated hydroxides were prepared in three ways; by homogenous precipitation of $TiCl_4$ and $ZrOCl_2 \cdot 8H_2O$ with urea, by direct addition of ammonium hydroxide to $TiCl_4$ and $ZrOCl_2 \cdot 8H_2O$ and by hydrolysis of metal alcoxides (titanium (IV) butoxide and zirconium *n*-propoxide in *n*-propanol). Maity et al. [4] and Reddy et al. [5] described the synthesis of $TiO_2$–$ZrO_2$ by homogenous precipitation method. $TiCl_4$, $ZrOCl_2 \cdot 8H_2O$ and urea were used as starting materials. Subsequently, the reaction products were calcined. Wu et al. [6] prepared catalysts from anhydrous alcohol solution containing equal moles of $TiCl_4$ and $ZrCl_4$ by adding 28% aqueous solution of ammonia. This catalyst was calcined at temperatures between 550 and 1,000 °C. Wang et al. [7] prepared samples of Zr-doped $TiO_2$ by the sol–gel method using $Ti(OC_4H_9)_4$ and $ZrOCl_2$ as starting materials. Manríquez et al. [8] prepared $TiO_2$–$ZrO_2$ mixed oxides by the sol–gel method under controlled pH conditions. Secar et al. [9] synthesized titanyl and zirconyl hydrazine carboxylates and their solid-solution precursors which decompose below 300 °C.

Improved photocatalytic properties of Zr-doped nanoparticulated $TiO_2$ were recently described in several papers [10–16]. The significant effect of low concentrations of Zr

J. Lukáč (✉) · M. Klementová · P. Bezdička · S. Bakardjieva · J. Šubrt · L. Szatmáry
Institute of Inorganic Chemistry of the ASCR, v.v.i., Husinec-Rez 25068, Czech Republic
e-mail: lukacj@iic.cas.cz

A. Grusková
Department of Electrotechnology, Faculty of Electrical Engineering and Information Technology, Slovak University of Technology, Ilkovičova 3, Bratislava 81219, Slovak Republic

in $TiO_2$ nanoparticulate powder or nanostructured films on photocatalytical activity of these materials is mostly believed to prevent particle sintering and to optimize pore structure during necessary thermal treatment. The increase of the anatase-rutile phase transformation temperature is also mentioned as a possible explanation of the enhancing effect of Zr on the photocatalytic activity of annealed materials. However, in order to synthesise active photocatalyst based on zirconium-doped titania, we need a starting material, amorphous or nanocrystalline, consisting of a very intimate mixture of Ti and Zr oxide components. Modifications of the sol–gel method as well as hydrothermal procedures are often used to prepare such mixtures [7, 8]. However, both these methods are rather expensive and potentially environmentally harmful. All the authors [3–9] described the preparation of Zr-doped $TiO_2$ by thermal treatment of precursors. Homogeneous precipitation of acid aqueous solutions of $TiOSO_4$ with urea is a cheap and ecologically safe method to synthesise nanocrystalline titanium oxide nanoparticles [17, 18]. In the present study, we used this method to synthesize $TiO_2$ nanocrystallites doped with different Zr contents (0–10 mol.%) and studied the relationship between the conditions of synthesis and the crystallite size, specific surface area, pore size distribution and morphology of porous titanium dioxide doped with zirconium.

## Experimental

### Synthesis

First, two solutions were prepared: (1) 100 g of $TiOSO_4 \times H_2O$ was dissolved in 300 mL of hot water acidified with 30 mL of 96% $H_2SO_4$, (2) zirconium tetrachloride $ZrCl_4$ was dissolved in 96% $H_2SO_4$ (see Table 1 for details on sample charges). Second, the two solutions were mixed together and water was added to reach final volume of 4 L. Subsequently, 250 g of urea (99.5% purity) was added into the solution to act as the precipitation agent. The gradual decomposition of urea at 70–80 °C homogenously raises the pH of an aqueous solution by releasing ammonium ions, and thus suppresses the rapid precipitation [19]. Urea was added each hour until the pH stabilized at 7. The experiment was carried out in a 4 L glass vessel at 98 °C, under constant stirring, for a minimum of 7 h (Table 1). The final co-precipitate was filtered, washed with distilled water and dried at 105 °C for approximately 12 h.

Sample preparation procedure is outlined in the flow chart (Fig. 1) and the reaction conditions are summarized in Table 1.

**Table 1** Experimental conditions and reactant charges used for synthesis of samples T/Z(0)–T/Z(20)

| Sample | Precipitation time [h] | $ZrCl_4$ [g] | $H_2SO_4$ [mL] | Urea [g] |
|---|---|---|---|---|
| T/Z(0) | 6 | 0 | 0 | 250 |
| T/Z(4) | 7 | 18 | 100 | 250 |
| T/Z(8) | 10 | 35 | 200 | 900 |
| T/Z(12) | 12 | 53 | 300 | 900 |
| T/Z(16) | 12 | 70 | 400 | 1,100 |
| T/Z(18) | 14 | 79 | 450 | 1,400 |
| T/Z(20) | 16 | 88 | 500 | 1,500 |

### Analytical methods

X-Ray powder diffraction was performed on a Siemens D5005 diffractometer (Bruker AXS, Germany) using Cu Kα radiation (40 kV, 30 mA) and a diffracted beam monochromator. Data were collected from 5° to 90° in a step-scan mode (step 0.02°, time per step 2.4 s). Qualitative phase analysis was performed with HighScore software package (PANalytical, the Netherlands, version 1.0d), Diffrac-Plus software package (Bruker AXS, Gernamy, version 8.0), and JCPDS PDF-2 database [20]. For quantitative phase analysis, Diffrac-Plus Topas software package (Bruker AXS, Germany, version 2.1) with structural models based on ICSD database [21] was used.

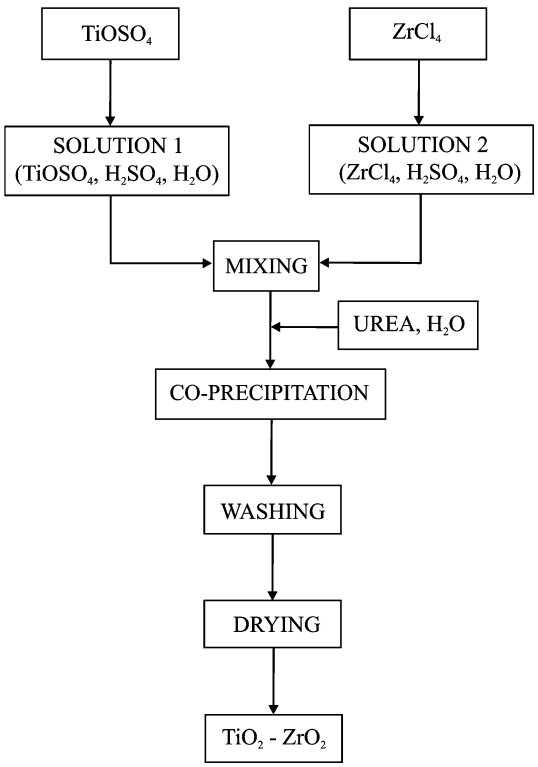


**Fig. 1** Flow diagram of sample preparation of Zr-doped $TiO_2$

Structural morphology of the samples was revealed by SEM (scanning electron microscopy). A Philips XL30 CP microscope equipped with EDX (Energy Dispersive X-ray), Robinson, SE (Secondary Electron) and BSE (Back Scattered Electron) detectors. The EDX information is correct to about ±3%.

Transmission electron microscopy (TEM) was carried out on a JEOL JEM 3010 microscope operated at 300 kV (point resolution 1.7 Å) with an EDX (Energy Dispersive X-ray) detector attached. Samples were reground in agate mortar, the powder was dispersed in ethanol and the suspension was treated in ultrasound for 10 min. A drop of very dilute suspension was placed on a carbon-coated grid and allowed to dry by evaporation at ambient temperature. Electron diffraction patterns were evaluated using the Process Diffraction software package [22].

The specific surface area of the samples was determined by nitrogen adsorption-desorption isotherms at liquid nitrogen temperature using the Coulter SA 3100 instrument with 15-min outgas at 120 °C. The specific surface area was calculated by the BET (Brunauer–Emmett–Teller) method. Pore size distribution was measured from the $N_2$ desorption isotherm using cylindrical pore model (BJH—Barret–Joyner–Halanda). The samples were outgassed for 30 min at 120 °C.

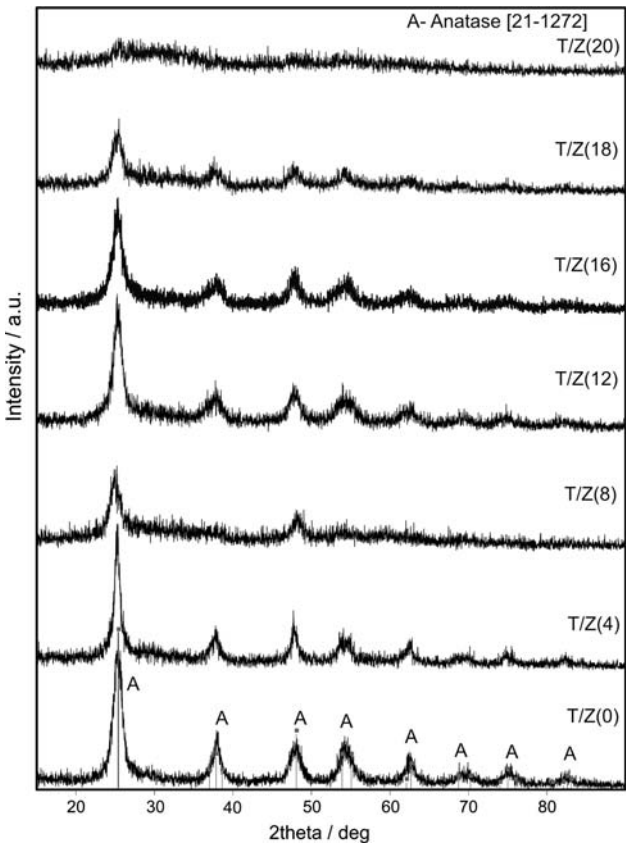


**Fig. 2** X-ray powder diffraction patterns of the samples T/Z(0), T/Z(4), T/Z(8), T/Z(12), T/Z(16), T/Z(18), and T/Z(20)

## Results and discussion

### X-ray powder diffraction (XRD)

The XRD patterns of Zr-doped $TiO_2$ nanocrystals are shown in Fig. 2. All correspond to anatase structure (ICDD PDF [20] card 21-1272), with a dominant 011 diffraction line at 25.01° 2Θ, except catalyst T/Z(8), which most probably corresponds to titanium hydrogen oxide $H_2Ti_8O_{17}$ (ICDD PDF [19] card 36-0656) with a dominant diffraction line at 23.57° 2Θ. Incomplete crystallization of sample T/Z(8) may have been caused by inadequate time needed for better crystallization at the same pH = 7. A diffusion maximum at around 30° 2Θ hints at the presence of amorphous phase in all samples. The intensities of anatase diffraction lines decrease with increasing Zr concentration (Fig. 2) as does the crystallite size (Table 2). Concomitant diffraction line broadening may be due to a fine nature of crystallites. Finally, sample T/Z(20) has mostly amorphous character.

Calculated lattice parameters are presented in Table 2. Due to the difference in ionic radii of zirconium and titanium ($Zr^{4+}$ = 72 pm, $Ti^{4+}$ = 61 pm [23]), increasing concentration of zirconium in the structure of anatase is expected to lead to a growth of lattice parameters and introduction of lattice deformations as reported by Wang et al. [7] and Lukac et al. [24]. However, it appears that in this case increasing Zr content does not have a profound effect on anatase lattice parameters, which suggest that Zr is only partially incorporated into the anatase structure while the rest of it concentrates in the amorphous phase. Nevertheless, the limited substitution of Zr ions for Ti ions might create some structural defects, such as vacancies, mainly on the surface to partially compensate the lattice strain [13].

### Cluster morphology and the effects of preparation

Figure 3 presents SEM micrographs of pure $TiO_2$ and Zr-doped $TiO_2$ grown by precipitation. Measured contents of Zr for all prepared samples by EDX spectrometry are listed in Table 2. In addition, the EDX spectra show that in all samples sulphate and chloride ions are absent. As it has been shown earlier [18], the urea precipitation method leads to the formation of colloid nanoparticles assembled in 1–2 μm porous spherical clusters. Particles in some regions of the clusters are submicron-scale balls, consisting of densely packed smaller particles. The clusters are spherical in shape and uniform in size. Structural changes in the material, e.g., growth of anatase nanocrystals and change of porosity, take

**Table 2** Results obtained by characterization of samples T/Z(0)–T/Z(20)—percentage content of Zr in $TiO_2$ (from EDS), cluster size (from SEM, TEM), crystallite size (from XRD, TEM), specific surface area (from BET) and lattice parameters (from XRD)

| Sample | Zr [mol.%] | Cluster size (μm) | Crystallite size (nm) | Surface area—BET [$m^2\ g^{-1}$] | Lattice parameters [Å] | |
|---|---|---|---|---|---|---|
| | | | | | *a* | *c* |
| T/Z(0) | 0 | 2 | 8.7 | 391.3 | 3.794 | 9.482 |
| T/Z(4) | 2.5 | 3–4 | 8.2 | 618.2 | 3.785 | 9.505 |
| T/Z(8) | 5.1 | 3–4 | 8.0 | 660.7 | – | – |
| T/Z(12) | 6.4 | 6–7 | 7.6 | 493.8 | 3.784 | 9.495 |
| T/Z(16) | 7.5 | 2–8 | 6.4 | 506.5 | 3.790 | 9.487 |
| T/Z(18) | 8.1 | 4–15 | 7.7 | 516.2 | 3.780 | 9.466 |
| T/Z(20) | 10.2 | 3–10 | – | 689.1 | – | – |

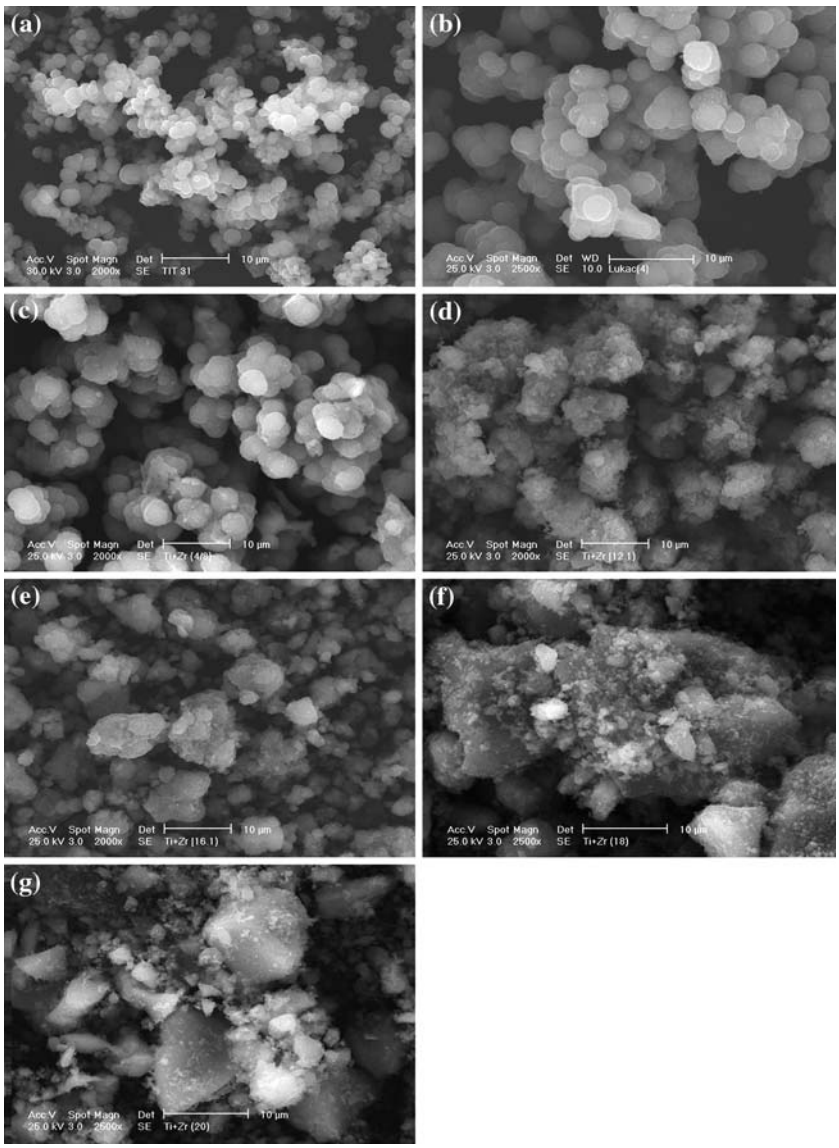


**Fig. 3** SEM images of the samples: (**a**) T/Z(0), (**b**) T/Z(4), (**c**) T/Z(8), (**d**) T/Z(12), (**e**) T/Z(16), (**f**) T/Z(18) and (**g**) T/Z(20)

place inside the clusters. Samples T/Z(0), T/Z(4) and T/Z(8) are uniform in morphology, with spherical shape and size of 3–4 μm. All other samples, T/Z(12), T/Z(16), T/Z(18), T/Z(20), are irregular in shape, and their size ranges from 6 to 15 μm. However, samples T/Z(12) and T/Z(16) show small areas with spherical shape clusters. Samples T/Z(18) and

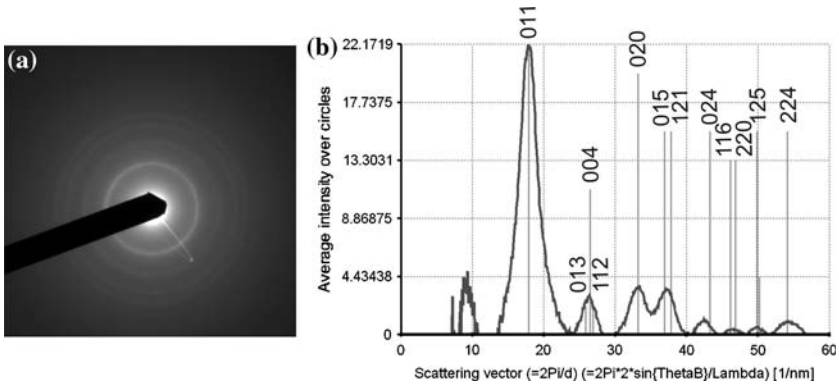


**Fig. 4** Electron diffraction of sample T/Z(12): (**a**) diffractogram, (**b**) electron diffraction pattern processed in Process Diffraction with markers indicating position of diffraction lines of anatase

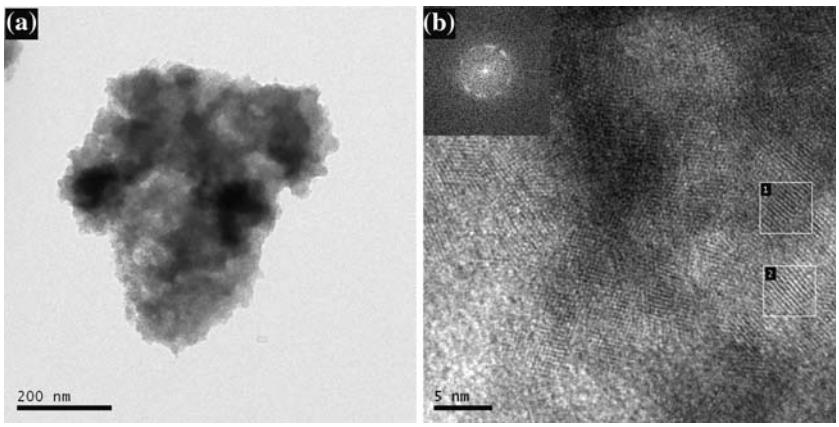


**Fig. 5** HRTEM observations of sample T/Z(12): (**a**) a cluster of anatase crystallites, (**b**) high-resolution image of anatase crystallites (inset—FFT of the whole image)

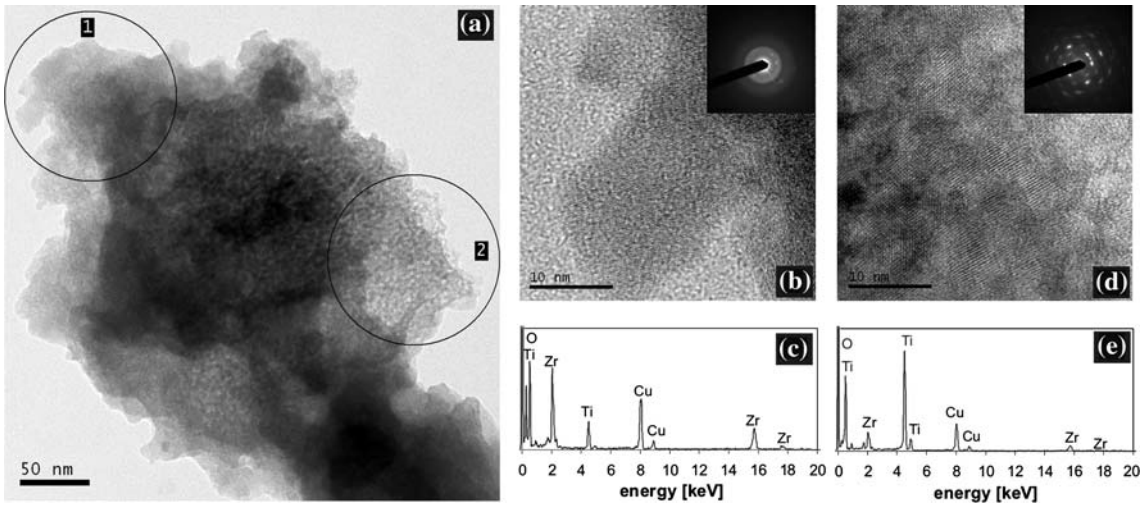


**Fig. 6** TEM observations of sample T/Z(8): (**a**) image of a cluster composed of two phases, (**b**) high-resolution image of area 1 (inset—electron diffraction from area 1 corresponding to amorphous phase), (**c**) EDX analysis from area 1, (**d**) high-resolution image of area 2 (inset—electron diffraction from area 1 corresponding to anatase) and (**e**) EDX analysis from area 2

T/Z(20) are conspicuous by their irregular morphology. We assume that the clusters consist of anatase nanoparticles interlaid by a small fraction of amorphous material. Small amount of Zr doping in $TiO_2$ (up to 5.1 mol.%) leads to the formation of spherical clusters, while elevated Zr doping causes the growth of irregular clusters. The different morphology of particles (clusters) may be explained by adsorption of sulphate anions on solid surface [19].

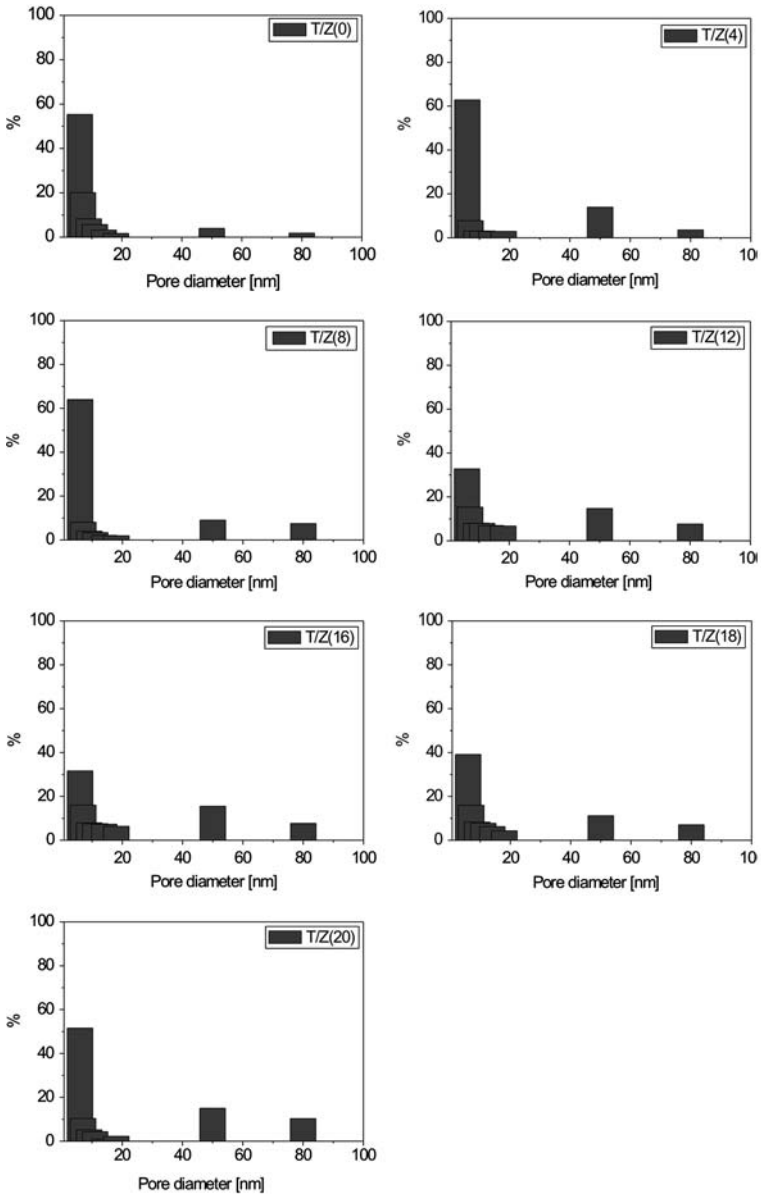


**Fig. 7** Pore size distribution of samples T/Z(0), T/Z(4), T/Z(8), T/Z(12), T/Z(16), T/Z(18), and T/Z(20)

High-resolution transmission electron microscopy (HRTEM) was used to close up on the phase composition and microstructure of the samples T/Z(12) and T/Z(8). In sample T/Z(12), electron diffraction confirms that the only crystalline phase present in the sample is anatase (Fig. 4). Fine-grained anatase crystallites closely intertgrown with amorphous phase form clusters (Fig. 5a, b). The size of individual crystallites is about 6 nm (Fig. 5b), which closely corresponds to the size of crystallites derived from XRD patterns (Table 2). In Fig. 5b, lattice fringes corresponding to anatase are observed. Namely, the lattice fringes of the area 1 and 2 have spacing of 3.52 Å corresponding to (011) lattice planes of anatase. In fact, when the FFT (Fast Fourier Transform) is applied to the whole image, it can be observed that all the lattice fringes on the image represent (011) lattice planes of anatase (Fig. 5). On the contrary, sample T/Z(8) appears very inhomogeneous (Fig. 6). It consists of areas containing amorphous (Zr > Ti)$O_2$, such as area 1 in Fig. 6a (enlarged in Fig. 6b, EDS analysis in Fig. 6c), as well as areas containing finely crystalline Zr-doped anatase, such as area 2 in Fig. 6a (enlarged in Fig. 6d, EDS analysis in Fig. 6e). The inhomogeneity of the sample is also reflected by the XRD data, which are anomalous, compared to the other samples. This was probably caused by imperfect, incomplete precipitation.

*Effect of aging time and concentration of reagents*

It is well known that temperature governs particle generation and crystal growth rate. The rate of precipitation obviously increases at a higher temperature. The crystal shape, size and morphology may also change with

temperature [25]. In the present case, conditions of precipitation lead to the generation of either uniform, spherical clusters of nanocrystallites and/or irregular clusters. Spherical clusters result from isotropic aggregation while irregular clusters are a consequence of oriented aggregation [26]. It was observed that precipitation time influences the formation process of Zr-doped $TiO_2$ nanocrystallite clusters (Table 1, Fig. 3). During the preparation of precursors, the temperature and the rate of stirring were constant. Therefore it was concluded that the effect of aging time, concentration of $ZrCl_4$, concentration of urea and concentration of sulphuric acid are the factors responsible for the change in morphology. At higher concentrations of reactants irregular shape of clusters is observed rather than spherical (Table 2).

### Specific surface area and porosity

The specific surface areas are listed in Table 2. BET surface area of pure anatase sample T/Z(0) has been determined as 391.3 $m^2\ g^{-1}$ which confirms the results of Wang et al. [7], who noticed that the BET surface area of pure $TiO_2$ is lower than that of mixed oxides. The homogenous co-precipitation method leads to high specific surface area. This is expected since the hydrosol is formed with a minimum of local hydroxide ion concentration gradient and this reduction in concentration gradients permits the growth of smaller crystals [3]. With the addition of zirconium to titania, the surface area of the resulting oxide increases sharply (from 391.3 to 689.1 $m^2\ g^{-1}$). The observed significant changes could be due to strong mutual interaction between titanium and zirconium oxides when precipitated together, which inhibits their individual crystallization [27]. The specific surface area correlates with the content of Zr in anatase. Let it be stressed that the highest surface area among the binary samples was observed in the amorphous sample T/Z(20).

It is well known that micropores have pore sizes from 0.3 to 2 nm. Mesopore substances have pore sizes from 2 up to 50 nm, and the sizes of macropores range from 50 nm up to about $10^5$ nm [28]. In samples T/Z(0), T/Z(4) and T/Z(8), the pore size distributions show that the total surface area is mainly attributed to micropores (Fig. 7), while the specific surface area increases gradually. It is likely that these micropores are present inside the spherical clusters nanocrystals. In the other samples, macropores are dominant.

## Conclusions

Zr-doped $TiO_2$ nanopowders have been successfully prepared by homogenous co-precipitation and characterized by several analytical methods. The following conclusions can be drawn: (i) X-ray powder diffraction and transmission electron microscopy detect polycrystalline anatase structure mixed with amorphous phase in all samples, except in the Zr-richest sample (10 mol.% Zr) which is amorphous. (ii) Scanning electron microscopy shows that samples with Zr content lower than 5.1 mol.% develop a uniform spherical morphology of the clusters whereas the irregular cluster morphology is observed at higher Zr contents. (iii) The BET surface area of pure $TiO_2$ is lower than that of the Zr-doped oxides. (iv) The BJH measurements show that samples with Zr content lower than 5.1 mol.% Zr contain dominantly micropores whereas samples with higher Zr contents are mainly mesoporous.

**Acknowledgements** This work was supported by the Academy of Sciences of the Czech Republic (Project No. AV OZ 40320502) and by the Ministry of Education of the Czech Republic (Project No. 1M4531477201).

## References

1. Das D, Mishra HK, Parida KM, Dalai AK (2002) J Mol Catal Chem 189:271
2. Aiken B, Hsu WP, Matijevic E (1990) J Mater Sci 25:1886
3. Daly FP, Ando H, Schmitt JL, Sturm EA (1987) J Catal 108:401
4. Maity SK, Rana MS, Bej SK, Juarez JA, Dhar GM, Rao TSRP (2001) Catal Lett 72:115
5. Reddy BM, Chowdhury B, Smirniotis PG (2001) Appl Catal Gen 211:19
6. Wu J-CH, Chung CH-S, Ay CH-L, Wang I (1984) J Catal 87:98
7. Wang YM, Liu SW, Lu MK, Wang SF, Gu F, Gai XZ, Cui XP, Pan J (2004) J Mol Catal Chem 215:137
8. Manriquez ME, Lopez T, Gomez R, Navarette J (2004) J Mol Catal Chem 220:229
9. Sekar MMA, Patil KC (1993) Mater Res Bull 28:485
10. Fu XZ, Clark LA, Yang Q, Anderson MA (1996) Environ Sci Tech 30:647
11. Gnatyuk Y, Smirnova N, Eremenko A, Ilyin V (2005) Adsorp Sci Technol 23:497
12. Hirano M, Nakahara C, Ota K, Inagaki M (2002) J Am Ceram Soc 85:1333
13. Hirano M, Nakahara C, Ota K, Tanaike O, Inagaki M (2003) J Solid State Chem 170:39
14. Schattka JH, Shchukin DG, Jia JG, Antonietti M, Caruso RA (2002) Chem Mater 14:5103
15. Tibbitts TW, Cushman KE, Fu X, Anderson MA, Bula RJ (1998) Adv Space Res 22:1443
16. Zhang YH, Xiong GX, Yao N, Yang WS, Fu XZ (2001) Catal Today 68:89
17. Stengl V, Subrt J, Bezdicka P, Marikova M, Bakardjieva S (2003) In: Diffusion and defect data, solid state data—part B: solid state phenomena. Scitec Publications, Switzerland, p 121
18. Bakardjieva S, Subrt J, Stengl V, Vecernikova E, Bezdicka P (2003) In: Diffusion and defect data, solid state data—part B: solid state phenomena. Scitec Publications, Switzerland, p 7
19. Yamabi S, Imai H (2003) Thin Solid Films 434:86
20. JCPDS PDF-2 release 2001, ICDD Newtown Square, PA, USA
21. ICSD Database FIZ Karlsruhe, Germany, 2005 (release 2005/1)
22. Labar JL (2002) Microsc Anal 21

23. Shannon RD, Prewitt CT (1969) Acta Crystallogr B25:925
24. Lukac J, Klementova M, Bezdicka P, Bakardjieva S, Subrt J, Szatmary L, Bastl Z, Jirkovsky J (2007) Appl Catal B Environ 74:83–91
25. Bakardjieva S, Stengl V, Subrt J, Vecernikova E (2005) Solid State Sci 7:367
26. Soler-Illia GJDAA, Jobbagy M, Candal RJ, Regazzoni AE, Blesa MA (1998) J Dispersion Sci Technol 19:207
27. Reddy BM, Khan A (2005) Catal Rev 47:257
28. IUPAC Manual of Symbols and Terminology (1972) Pure Appl Chem 31:578